Isolation, sequence, infectivity and replication kinetics of SARS-CoV-2

Arinjay Banerjee[1], Jalees A. Nasir[1], Patrick Budylowski[2], Lily Yip[3], Patryk Aftanas[3], Natasha Christie[2], Ayoob Ghalami[2], Kaushal Baid[1], Amogelang R. Raphenya[1], Jeremy A. Hirota[1], Matthew S. Miller[1], Allison J. McGeer[2,4], Mario Ostrowski[2], Robert A. Kozak[2,3], Andrew G. McArthur[1], Karen Mossman[1,*] and Samira Mubareka[2,3]

Affiliations:

[1]McMaster University, Hamilton, Ontario, Canada

[2]University of Toronto, Toronto, Ontario, Canada

[3]Sunnybrook Research Institute, Toronto, Ontario, Canada

[4]Mount Sinai Hospital, Toronto, Ontario, Canada

*Corresponding author:

Dr. Karen Mossman

Professor

McMaster University

1280 Main St. W

Hamilton L8S 4L8, Canada

Email: mossk@mcmaster.ca

ABSTRACT

SARS-CoV-2 emerged in December 2019 in Wuhan, China and has since infected over 1.5 million people, of which over 107,000 have died. As SARS-CoV-2 spreads across the planet, speculations remain about the range of human cells that can be infected by SARS-CoV-2. In this study, we report the isolation of SARS-CoV-2 from two cases of COVID-19 in Toronto, Canada. We determined the genomic sequences of the two isolates and identified single nucleotide changes in representative populations of our virus stocks. More importantly, we tested a wide range of human immune cells for productive infection with SARS-CoV-2. Here we confirm that human primary peripheral blood mononuclear cells (PBMCs) are not permissive for SARS-CoV-2. As SARS-CoV-2 continues to spread globally, it is essential to monitor single nucleotide polymorphisms in the virus and to continue to isolate circulating viruses to determine viral genotype and phenotype using *in vitro* and *in vivo* infection models.

Keywords: SARS-CoV-2, isolation, replication, immune cells, phylogenetics, COVID-19

TEXT

A new coronavirus, severe acute respiratory syndrome coronavirus 2 (SARS-CoV-2) emerged in December 2019 in Wuhan, China (1). SARS-CoV-2 has since spread to 185 countries and infected over 1.7 million people, of which over 107,000 have died (2). The first case of COVID-19 was detected in Toronto, Canada on January 23, 2020 (3). Multiple cases have since been identified across Canada. As SARS-CoV-2 spreads globally, the virus is likely to adapt and evolve. It is critical to isolate SARS-CoV-2 viruses to characterize their ability to infect and replicate in multiple human cell types and to determine if the virus is evolving in its ability to infect human cells and cause severe disease. Isolating the virus also provides us with the

47 opportunity to share the virus with other researchers to facilitate the development and testing of
48 diagnostics, drugs and vaccines.
49
50 In this study, we describe how we isolated and determined the genomic sequence of SARS-CoV-
51 2 from two cases of COVID-19 (SARS-CoV-2/SB2 and SARS-CoV-2/SB3-TYAGNC). In
52 addition, we studied the replication kinetics of SARS-CoV-2/SB3-TYAGNC in human
53 fibroblast, epithelial and immune cells. Importantly, we report that although a human lung cell
54 line supported SARS-CoV-2 replication, the virus did not propagate in any of the tested immune
55 cell lines or primary human immune cells. Interestingly, although we did not observe a
56 productive infection in $CD4^+$ primary T cells, we observed virus-like particles in these cells by
57 electron microscopy. Our data shed light on a wider range of human cells that may or may not be
58 permissive for SARS-CoV-2 replication and our studies strongly suggest that the human immune
59 cells tested do not support a productive infection with SARS-CoV-2. Further studies are required
60 to understand viral-host dynamics in immune cells.

61 **METHODS**

62 **Cells**

63 Vero E6 cells (African green monkey cells; ATCC, https://www.atcc.org) were maintained in
64 Dulbecco's modified Eagle's media (DMEM) supplemented with 10% fetal bovine serum (FBS;
65 Sigma-Aldrich, https://www.sigmaaldrich.com), 1x L-Glutamine and Penicillin/Streptomycin
66 (Pen/Strep; Corning, https://ca.vwr.com). Calu-3 cells (human lung adenocarcinoma derived;
67 ATCC, https://www.atcc.org) were cultured as previously mentioned (4). THF cells (human
68 telomerase life-extended cells) were cultured as previously mentioned (5). THP-1 cells
69 (monocytes; ATCC, https://www.atcc.org) were cultured in RPMI media (Gibco,

70 https://www.thermofisher.com) supplemented with 10% FBS, 2mM L-glutamine, 1x
71 Penicillin/streptomycin and 0.05 mM beta-mercaptoethanol. THP-1 cells were differentiated into
72 macrophages and dendritic cells using 50 ng/ml GM-CSF (R&D Systems,
73 https://www.rndsystems.com) + 50 ng/ml M-CSF (R&D Systems, https://www.rndsystems.com)
74 and 50 ng/ml GM-CSF + 500 U/ml IL-4 (Biolegend, https://www.biolegend.com), respectively.
75 PBMCs from healthy donors (n=2; OM8066 and OM8067) were purified into $CD4^+$, $CD8^+$,
76 $CD19^+$, monocytes and others ($CD4^-$ $CD8^-$ $CD19^-$ cells) using CD4 negative selection kit
77 (STEMCELL Technologies, https://www.stemcell.com), CD8 positive selection kit
78 (STEMCELL Technologies, https://www.stemcell.com), PE positive selection kit (STEMCELL
79 Technologies, https://www.stemcell.com) and Monocyte negative selection kit (STEMCELL
80 Technologies, https://www.stemcell.com), respectively. For purity of cell types, see
81 supplementary figure 1. $CD4^+$, $CD8^+$, $CD19^+$ and $CD4^-$ $CD8^-$ $CD19^-$ cells were resuspended in
82 R-10 media (RPMI + 2 mM L-glutamine + 10% FBS + Penicillin/streptomycin) + 20 U/ml IL-2
83 (Biolegend, https://www.biolegend.com). Primary monocytes were resuspended in R-10 media.
84 This work was approved by the Sunnybrook Research Institute Research Ethics Board (149-
85 1994) and the Research Ethics Boards of St. Michael's Hospital and the University of Toronto
86 (REB 20-044; for PBMCs).

87 **Virus isolation and quantification**

88 Vero E6 cells were seeded at a concentration of $3x10^5$ cells/well in a 6-well plate. Next day,
89 200 µl of mid-turbinate swabs, collected from two COVID-19 patients was mixed with 200 µl of
90 DMEM containing 16 µg/ml TPCK-treated trypsin and cells were inoculated. After 1 hr, the
91 inoculum was replaced with DMEM containing 2% FBS and 6 µg/ml TPCK-treated trypsin. The
92 cells were observed daily under a light microscope. Supernatant from the cells were used to

93 determine virus titres ($TCID_{50}$/ml) using Spearman and Karber's method (6, 7) as outlined
94 previously (8).

95 **Quantitative real time PCR**

96 To detect SARS-CoV-2 in cell culture supernatant, 140 uL of supernatant was removed and
97 detection of viral nucleic acids was performed by RT-PCR using an adaptation of Corman *et*
98 *al.'s* protocol (9). Briefly, viral RNA was extracted from infected cells using QIAamp viral RNA
99 kit (Qiagen, https://www.qiagen.com) according to manufacturer's instructions. The RT-PCR
100 reactions were carried out using Luna Universal qPCR Master Mix (New England Biolabs,
101 https://www.neb.ca) according to manufacturer's instructions. Two separate gene targets were
102 used for detection, the 5' untranslated region (UTR) and the envelope (E) gene. Primers and
103 probes used were: 5'-UTR For: GTTGCAGCCGATCATCAGC; 5'-UTR Rev:
104 GACAAGGCTCTCCATCTTACC; 5'-UTR probe: FAM-
105 CGGTCACACCCGGACGAAACCTAG-BHQ-1; E-gene For:
106 ACAGGTACGTTAATAGTTAATAGCGT; E-gene Rev: ATATTGCAGCAGTACGCACACA;
107 E-gene probe: CAL Fluor Orange 560-ACACTAGCCATCCTTACTGCGCTTCG-BHQ-1. The
108 cycling conditions were: 1 cycle of denaturation at 60°C for 10 minutes then 95°C for 2 minutes
109 followed by 44 amplification cycles of 95°C for 10s and 60°C for 15s. Analysis was performed
110 using the Rotor-Gene Q software (Qiagen, https://www.qiagen.com) to determine cycle
111 thresholds (Ct).

112 **Electron Microscopy**

113 Samples were fixed in 10% neutral buffered formalin (Sigma-Aldrich,
114 https://www.sigmaaldrich.com/) for 1 hr. Pellets were washed with 0.1 M phosphate buffer (pH
115 7.0) and post-fixed with 1% osmium tetroxide in 0.1 M phosphate buffer (pH 7.0) for 1 hr.

116 Pellets were washed with distilled water and en-bloc stained with 2% uranyl acetate in distilled
117 water for 2 hrs. Pellets were washed with distilled water and dehydrated in an ethanol series.
118 Pellets were infiltrated with Embed 812/Araldite resin and cured at 65 degrees for 48 hrs. Resin
119 blocks were trimmed, polished and 90 nm thin sections were ultramicrotomed (Leica Reichert
120 Ultracut E, https://www.leica-microsystems.com) and mounted on TEM grids. Thin sections
121 were stained with 5% uranyl acetate and 5% lead citrate. Sections were imaged using
122 Transmission Electron Microscopy (ThermoFisher Scientific Talos L120C,
123 https://www.thermofisher.com) using a LaB6 filament at 120kV. 10 fields per cell type were
124 scanned. Each field was imaged with different magnifications at 2600x, 8500x, 17500x and
125 36000x.

126 **Flowcytometry**

127 To prepare cells for flowcytometry, 100µL (400,000 cells) of primary $CD4^+$, $CD8^+$, $CD19^+$ and
128 monocytes were washed with 1 ml of phosphate buffered saline (PBS) and spun at 500 g for 5
129 minutes. The cells were resuspended in 100 µL of Live/Dead Violet (ThermoFisher Scientific,
130 https://www.thermofisher.com) as per manufacturer's recommendation and diluted 1:1000 in
131 PBS. Cells were incubated at 4°C for 30 minutes. Next, cells were washed with 1 ml of FACS
132 buffer (in-house reagent) and spun at 500 g for 5 minutes. Cells were then stained with 100 µL of
133 their respective stains (αCD4-FITC, αCD8-FITC, αCD19-FITC, αCD14-APC; Biolegend,
134 https://www.biolegend.com) at a concentration of 1µg/mL for 30 min at 4°C. After staining, the
135 cells were washed with 1mL of FACS Buffer and spun at 500 g for 5 minutes. Extra aliquots of
136 cells were left unstained, which were also spun at 500g for 5 minutes. The pellets were
137 resuspended in 100 µL of 1% paraformaldehyde (PFA; ThermoFisher Scientific,
138 https://www.thermofisher.com) and analyzed. Samples were run on the BD LSR Fortessa X20

139 (BD, https://www.bdbiosciences.com). Cells were gated on Live/Dead negative to exclude debris
140 and dead cells and were then gated on their respective cell surface markers to assess purity.
141 **Sequencing**
142 RNA was extracted from the supernatant of Vero E6 cells after 1 passage using the QIAamp
143 Viral RNA Mini kit (Qiagen, https://www.qiagen.com/us/) without addition of carrier RNA.
144 dsDNA for sequencing library preparation was synthesized using the Liverpool SARS-CoV-2
145 amplification protocol (10). Two 100 µM primer pools were prepared by combining primer pairs
146 in an alternating fashion to prevent amplification of overlapping regions in a single reaction. In a
147 PCR tube, 1µL Random Primer Mix (ProtoScript II First Strand cDNA Synthesis Kit, New
148 England Biolabs, https://www.neb.ca) was added to 7 µL extracted RNA and denatured on
149 SimpliAmp thermal cycler (ThermoFisher Scientific, https://www.thermofisher.com) at 65°C for
150 5 min and then incubated on ice. 10 µL 2X ProtoScript II Reaction Mix and 2 µL 10X
151 ProtoScript II Enzyme Mix were then added to the denatured sample and cDNA synthesis
152 performed using the following conditions: 25°C for 5 min, 48°C for 15 min and 80°C for 5 min.
153 After cDNA synthesis, in a new PCR tube 2.5 µL cDNA was combined with 12.5 µL Q5 High-
154 Fidelity 2X Master Mix (NEB, Ipswich, USA), 8.8 µL nuclease free water (ThermoFisher
155 Scientific, https://www.thermofisher.com), and 1.125 µL of 100 µM primer pool #1 or #2. PCR
156 cycling was then performed as follows: 98°C for 30 sec followed by 40 cycles of 98°C for 15 sec
157 and 65°C for 5 min.
158
159 All PCR reactions were purified using RNAClean XP (Beckman Coulter,
160 https://www.beckmancoulter.com) at 1.8x bead to amplicon ratio and eluted in 30 µL. 2 µL of
161 amplified material was quantified using a Qubit 1X dsDNA (ThermoFisher Scientific,

162 https://www.thermofisher.com) following the manufacturer's instructions. Illumina sequencing
163 libraries were prepared using Nextera DNA Flex Library Prep Kit and Nextera DNA CD Indexes
164 (Illumina, https://www.illumina.com) according to manufacturer's instructions. Paired-end 150
165 bp sequencing was performed for each library on a MiniSeq with the 300-cycle mid-output
166 reagent kit (Illumina, https://www.illumina.com), multiplexed with targeted sampling of ~40,000
167 clusters per library. Sequencing reads from pool #1 and pool #2 were combined (as R1 and R2),
168 amplification primer sequences removed using cutadapt (version 1.18) (11), and Illumina adapter
169 sequences were removed and low quality sequences trimmed or removed using Trimmomatic
170 (version 0.36) (12). Final sequence quality and confirmation of adapter/primer trimming were
171 confirmed by FASTQC (version 0.11.5) (13). SARS-CoV-2 genome sequences were assembled
172 using UniCycler (version 0.4.8; default settings, except for --mode conservative) (14) and
173 assembly statistics generated by QUAST (version 5.0.2) (15). Sequencing depth and
174 completeness of coverage of the assembled genomes was additionally assessed by Bowtie2
175 (version 2.3.4.1) (16) alignment of the sequencing reads against the assembled contigs and
176 statistics generated by ngsCAT (version 0.1) (17). Sequence variation in the assembled genomes
177 was assessed by BLASTN against SARS-CoV-2 genome sequences available in GenBank as
178 well as BreSeq (version 0.35.0) (18) analysis relative to GenBank entry MN908947.3 (first
179 genome sequence reported from the original Wuhan outbreak, China).
180

181 **RESULTS**

182 For virus isolation, we inoculated Vero E6 cells with the samples collected from mid-turbinate
183 swabs and monitored for cytopathic effects (CPE) daily. Seventy-two hours post infection (hpi),
184 cells inoculated with both samples displayed extensive CPE, relative to mock-inoculated cells

185 (Figure 1, panel A). We collected 200 uL of cell culture supernatant and re-infected a fresh layer
186 of Vero E6 cells. Twenty-four hours post infection, both wells containing cells that were re-
187 inoculated displayed extensive CPE (Figure 1, panel B). We extracted viral RNA from the
188 supernatant and confirmed the presence of SARS-CoV-2 using a diagnostic real-time PCR assay
189 (qPCR; Figure 1, panel C). We also confirmed the presence of coronavirus-like particles in
190 infected Vero E6 cells by electron microscopy (Figure 1, panel D).
191
192 Next, we performed genome sequencing of both isolates, generating genome sequences with
193 7500-8000 fold coverage and ~94% completeness, with only ~260 bp and ~200 bp at the 5' and
194 3' termini undetermined (Table 1). Both shared synonymous and non-synonymous substitutions
195 with those independently observed in direct sequencing of clinical isolates (Table 1; Mubareka &
196 McArthur, unpublished). SARS-CoV-2/SB2 additionally contained a non-synonymous
197 substitution at position 2832 (K856R in ORF1ab polyprotein) and three regions with mutations
198 or a deletion supported by a minority of sequencing reads, while SARS-CoV-2/SB3-TYAGNC
199 only had an additional synonymous substitution in ORF1ab polyprotein (Y925Y) plus a minority
200 of sequencing reads supporting another synonymous substitution in the ORF3a protein (I7I). As
201 such, SARS-CoV-2/SB3-TYAGNC was used for subsequent studies as best representative of a
202 clinical viral isolate. Raw sequencing reads for each isolate are available in NCBI BioProject
203 PRJNA624792. Only sequencing reads that aligned by Bowtie2 to the MN908947.3 SARS-CoV-
204 2 genome were included in the deposited sequence files.
205
206 To determine the replication kinetics of SARS-CoV-2 in human structural and immune cells, we
207 infected Calu-3 (lung adenocarcinoma epithelial), THF (telomerase life extended human

208 fibroblasts), Vero E6 (African green monkey kidney epithelial), THP-1 (monocytes and
209 differentiated macrophages and dendritic cells) and primary peripheral blood mononuclear cells
210 (PBMCs) from healthy human donors ($CD4^+$, $CD8^+$, $CD19^+$, monocytes and other PBMCs;
211 Supplementary Figure S1) with a multiplicity of infection (MOI) of 0.01. We monitored virus
212 replication over a period of 72 hours in the cell lines (Figure 2). We also determined virus
213 replication in PBMCs from healthy donors over a period of 48 hours (Figure 2). SARS-CoV-2
214 propagated to high titres in Vero E6 and Calu-3 cells (Figure 2). SARS-CoV-2 did not replicate
215 efficiently in THF cells (Figure 2). Interestingly, human immune cell lines and primary PBMCs
216 from healthy donors did not support SARS-CoV-2 replication (Figure 2)
217
218 To further support virus replication data, we imaged infected human epithelial, fibroblast and
219 immune cells using electron microscopy after 48 hrs of infection with SARS-CoV-2 at a MOI of
220 0.01 (Figure 3). We scanned 10 different fields per cell type, each using four different
221 magnifications of 2600x, 8500x, 17500x and 36000x to determine if the cell populations
222 contained virus-like particles. Virus-like particles were detected in 7/10 fields in Vero E6 cells
223 and 8/10 fields in Calu-3 cells (Figure 3, panels A and B). Interestingly, we also detected virus-
224 like particles in 2/10 fields in primary $CD4^+$ T cells (Figure 3, panel C). We did not observe any
225 virus-like particles in other human immune cells that were experimentally infected with SARS-
226 CoV-2 (Figure 3, panels D-J).
227
228 **DISCUSSION**
229 In this study, we report the isolation of two replication competent SARS-CoV-2 isolates from
230 COVID-19 patients in Canada. We used TPCK-treated trypsin to enhance infection using clinical

231 specimens (Figure 1, panel A). Exogenous trypsin activates SARS-CoV spike proteins more
232 efficiently and facilitates cellular entry (19). Exogenous trypsin treatment has also been shown to
233 enhance infectivity of other zoonotic bat-borne coronaviruses (20). Furthermore, TPCK-treated
234 trypsin was used to successfully isolate SARS-CoV-2 in China (1). In our studies, subsequent
235 infection and virus replication did not require any additional TPCK-treated trypsin (Figure 1,
236 panel B). The presence of CPE alone does not indicate the successful isolation of a coronavirus.
237 Mid-turbinate samples from adults with acute respiratory distress may often contain other
238 microbes, including viruses (21). Thus, to identify our isolates, we sequenced them to confirm
239 that they were reflective of SARS-CoV-2 isolates infecting patients worldwide, selecting SARS-
240 CoV-2/SB3-TYAGNC for experimental investigation since this isolate produced less minority
241 sequencing reads (Table 1).
242
243 SARS-CoV caused the 2003-04 outbreak of SARS. SARS-CoV can infect structural (22) and
244 immune cell lines (23) from humans *in vitro*. We infected a range of human cell populations with
245 SARS-CoV-2/SB3-TYAGNC to identify cell types that can support productive infection of
246 SARS-CoV-2. Both Vero E6 and Calu-3 cells supported SARS-CoV-2 replication to high titres
247 (Figure 2), as reported in other recent studies (24, 25). Previously, SARS-CoV was also shown to
248 replicate efficiently in Vero E6 cells (22). Vero E6 cells are immunodeficient, with deficiencies
249 in innate antiviral interferon signaling, which makes them ideal candidates for virus isolation
250 (26). However, to enable studies on SARS-CoV-2-host interactions, it is important to identify
251 human lung epithelial cells with intact immune responses that can support SARS-CoV-2
252 replication. We and others have previously shown that SARS-CoV and Middle East respiratory
253 syndrome coronavirus (MERS-CoV) replicate efficiently in Calu-3 cells (8, 27, 28). In addition,

254 SARS-CoV- and MERS-CoV-induced immune responses have been studied in Calu-3 cells (28,
255 29). The ability to infect Calu-3 cells with SARS-CoV-2 (Figure 2) will facilitate *in vitro* studies
256 into virus-host interactions using SARS-CoV-2. Other commonly used human lung cells, such as
257 A549 do not support efficient replication of SARS-CoV-2 (24). Furthermore, hTERT life-
258 extended human fibroblast cells (THF) also did not support virus replication (Figure 2).
259
260 Previous studies have shown that human immune cells, such as THP-1 cell lines are susceptible
261 to SARS-CoV infection (23). In our study, human immune cell populations, including THP-1-
262 derived cell lines and primary cells (PBMCs) did not support productive SARS-CoV-2
263 replication (Figure 2). Interestingly, although primary $CD4^+$ T cells did not support productive
264 virus replication, we observed virus-like particles in these cells by electron microscopy (Figure
265 3, panel C). This is consistent with a recent report by Wang and colleagues where they
266 demonstrated that human T cell lines are susceptible to SARS-CoV-2 and pesudotyped viruses
267 (30). However, the study by Wang *et al.* did not quantify virus titres in the supernatant from
268 infected cells. In our study, we could not detect any replication competent virus in the
269 supernatant that was collected from SARS-CoV-2 infected $CD4^+$ T cells (Figure 3). Human
270 immune cells lack expression of angiotensin converting enzyme 2 (ACE2) (31)
271 (https://www.proteinatlas.org), the functional receptor of SARS-CoV-2 (1, 32). Thus, although it
272 is intriguing that $CD4^+$ T cells may be susceptible to SARS-CoV-2, our data show that these cells
273 are not permissive to SARS-CoV-2 replication *in vitro*.
274
275 In this study, we show that primary human T cells ($CD4^+$ and $CD8^+$) do not support productive
276 virus replication. However, our electron micrographs demonstrate that SARS-CoV-2 likely

277 replicates in $CD4^+$ T cells, but the replication cycle is likely terminated prior to virus maturation
278 and egress. Thus, more work is needed to fully identify the susceptibility and permissivity of
279 $CD4^+$ T cells to SARS-CoV-2.

280 **ACKNOWLEDGEMENTS**

281 We would like to acknowledge Lindsey Fiddes' help with electron microscopy. SARS-CoV-2
282 Liverpool protocol genome amplification primer sequences were generously shared by Public
283 Health England.
284
285 This study was supported by a Canadian Institutes of Health Research (CIHR) COVID-19 rapid
286 response grant to principal applicant K.M. and Co-Applicants A.B., A.G.M., M.S.M. and S.M.
287 A.B. is funded by the Natural Sciences and Engineering Research Council of Canada (NSERC).
288 J.A.N. was supported by funds from the Comprehensive Antibiotic Resistance Database. B.P.A.
289 and A.R.R. were supported by Canadian Institutes of Health Research (CIHR) funding (PJT-
290 156214 to A.G.M.). Computer resources were supplied by the McMaster Service Lab and
291 Repository computing cluster, funded in part by grants to A.G.M. from the Canadian Foundation
292 for Innovation. Additional cloud computing needs were funded by the Comprehensive Antibiotic
293 Resistance Database. J.A.H. is supported by the Canada Research Chairs Program and an
294 Ontario Early Career Researcher Award. M.S.M. is supported by a CIHR COVID-19 rapid
295 response grant, a CIHR New Investigator Award and an Ontario Early Researcher Award.
296
297
298
299

300 **REFERENCES**

301 1. Zhou P, Yang XL, Wang XG, Hu B, Zhang L, Zhang W, et al. A pneumonia outbreak
302 associated with a new coronavirus of probable bat origin. Nature. 2020 Feb 3.

303 2. Dong E, Du H, Gardner L. An interactive web-based dashboard to track COVID-19 in
304 real time. The Lancet Infectious Diseases. 2020.

305 3. Marchand-Senecal X, Kozak R, Mubareka S, Salt N, Gubbay JB, Eshaghi A, et al.
306 Diagnosis and Management of First Case of COVID-19 in Canada: Lessons applied from SARS.
307 Clin Infect Dis. 2020 Mar 9.

308 4. Aguiar JA, Huff RD, Tse W, Stampfli MR, McConkey BJ, Doxey AC, et al.
309 Transcriptomic and barrier responses of human airway epithelial cells exposed to cannabis
310 smoke. Physiol Rep. 2019 Oct;7(20):e14249.

311 5. Banerjee A, Zhang X, Yip A, Schulz KS, Irving AT, Bowdish D, et al. Positive Selection
312 of a Serine Residue in Bat IRF3 Confers Enhanced Antiviral Protection. iScience. 2020 Mar
313 2;23(3):100958.

314 6. Hamilton MA, Russo RC, Thurston RV. Trimmed Spearman-Karber method for
315 estimating median lethal concentrations in toxicity bioassays. Environmental Science &
316 Technology. 1977;11(7):714-9.

317 7. Spearman C. The Method of “Right and Wrong Cases” (Constant Stimuli) without
318 Gauss’s Formula. Br J Psychol. 1908;2:227-42.

319 8. Banerjee A, Falzarano D, Rapin N, Lew J, Misra V. Interferon Regulatory Factor 3-
320 Mediated Signaling Limits Middle-East Respiratory Syndrome (MERS) Coronavirus
321 Propagation in Cells from an Insectivorous Bat. Viruses. 2019 Feb 13;11(2).

322 9. Corman VM, Landt O, Kaiser M, Molenkamp R, Meijer A, Chu DKW, et al. Detection of
323 2019 novel coronavirus (2019-nCoV) by real-time RT-PCR. Euro Surveill. 2020 Jan;25(3).
324 10. Quick J, Grubaugh ND, Pullan ST, Claro IM, Smith AD, Gangavarapu K, et al. Multiplex
325 PCR method for MinION and Illumina sequencing of Zika and other virus genomes directly
326 from clinical samples. Nat Protoc. 2017 Jun;12(6):1261-76.
327 11. Martin M. Cutadapt removes adapter sequences from high-throughput sequencing reads.
328 EMBnetjournal. 2011;17(1).
329 12. Bolger AM, Lohse M, Usadel B. Trimmomatic: a flexible trimmer for Illumina sequence
330 data. Bioinformatics. 2014 Aug 1;30(15):2114-20.
331 13. Andrew S. FastQC: A Quality Control Tool for High Throughput Sequence Data
332 [Online]. 2010 [cited 2020 April 09]; Available from:
333 http://www.bioinformatics.babraham.ac.uk/projects/fastqc/
334 14. Wick RR, Judd LM, Gorrie CL, Holt KE. Unicycler: Resolving bacterial genome
335 assemblies from short and long sequencing reads. PLoS Comput Biol. 2017 Jun;13(6):e1005595.
336 15. Gurevich A, Saveliev V, Vyahhi N, Tesler G. QUAST: quality assessment tool for
337 genome assemblies. Bioinformatics. 2013 Apr 15;29(8):1072-5.
338 16. Langmead B, Salzberg SL. Fast gapped-read alignment with Bowtie 2. Nat Methods.
339 2012 Mar 4;9(4):357-9.
340 17. Lopez-Domingo FJ, Florido JP, Rueda A, Dopazo J, Santoyo-Lopez J. ngsCAT: a tool to
341 assess the efficiency of targeted enrichment sequencing. Bioinformatics. 2014 Jun
342 15;30(12):1767-8.
343 18. Deatherage DE, Barrick JE. Identification of mutations in laboratory-evolved microbes
344 from next-generation sequencing data using breseq. Methods Mol Biol. 2014;1151:165-88.

345 19. Simmons G, Bertram S, Glowacka I, Steffen I, Chaipan C, Agudelo J, et al. Different
346 host cell proteases activate the SARS-coronavirus spike-protein for cell-cell and virus-cell
347 fusion. Virology. 2011 May 10;413(2):265-74.
348 20. Menachery VD, Dinnon KH, 3rd, Yount BL, Jr., McAnarney ET, Gralinski LE, Hale A,
349 et al. Trypsin treatment unlocks barrier for zoonotic bat coronaviruses infection. J Virol. 2019
350 Dec 4.
351 21. Larios OE, Coleman BL, Drews SJ, Mazzulli T, Borgundvaag B, Green K, et al. Self-
352 collected mid-turbinate swabs for the detection of respiratory viruses in adults with acute
353 respiratory illnesses. PLoS One. 2011;6(6):e21335.
354 22. Kaye M. SARS-associated coronavirus replication in cell lines. Emerg Infect Dis. 2006
355 Jan;12(1):128-33.
356 23. Yen YT, Liao F, Hsiao CH, Kao CL, Chen YC, Wu-Hsieh BA. Modeling the early events
357 of severe acute respiratory syndrome coronavirus infection in vitro. J Virol. 2006
358 Mar;80(6):2684-93.
359 24. Harcourt J, Tamin A, Lu X, Kamili S, Sakthivel SK, Murray J, et al. Severe Acute
360 Respiratory Syndrome Coronavirus 2 from Patient with 2019 Novel Coronavirus Disease, United
361 States. Emerg Infect Dis. 2020 Mar 11;26(6).
362 25. Matsuyama S, Nao N, Shirato K, Kawase M, Saito S, Takayama I, et al. Enhanced
363 isolation of SARS-CoV-2 by TMPRSS2-expressing cells. Proc Natl Acad Sci U S A. 2020 Mar
364 31;117(13):7001-3.
365 26. Emeny JM, Morgan MJ. Regulation of the interferon system: evidence that Vero cells
366 have a genetic defect in interferon production. J Gen Virol. 1979 Apr;43(1):247-52.

367 27. Tseng CT, Tseng J, Perrone L, Worthy M, Popov V, Peters CJ. Apical entry and release
368 of severe acute respiratory syndrome-associated coronavirus in polarized Calu-3 lung epithelial
369 cells. J Virol. 2005 Aug;79(15):9470-9.
370 28. Lau SK, Lau CC, Chan KH, Li CP, Chen H, Jin DY, et al. Delayed induction of
371 proinflammatory cytokines and suppression of innate antiviral response by the novel Middle East
372 respiratory syndrome coronavirus: implications for pathogenesis and treatment. J Gen Virol.
373 2013 Dec;94(Pt 12):2679-90.
374 29. Yoshikawa T, Hill TE, Yoshikawa N, Popov VL, Galindo CL, Garner HR, et al.
375 Dynamic innate immune responses of human bronchial epithelial cells to severe acute respiratory
376 syndrome-associated coronavirus infection. PLoS One. 2010 Jan 15;5(1):e8729.
377 30. Wang X, Xu W, Hu G, Xia S, Sun Z, Liu Z, et al. SARS-CoV-2 infects T lymphocytes
378 through its spike protein-mediated membrane fusion. Cellular & Molecular Immunology. 2020.
379 31. Uhlen M, Fagerberg L, Hallstrom BM, Lindskog C, Oksvold P, Mardinoglu A, et al.
380 Proteomics. Tissue-based map of the human proteome. Science. 2015 Jan
381 23;347(6220):1260419.
382 32. Hoffmann M, Kleine-Weber H, Schroeder S, Krüger N, Herrler T, Erichsen S, et al.
383 SARS-CoV-2 Cell Entry Depends on ACE2 and TMPRSS2 and Is Blocked by a Clinically
384 Proven Protease Inhibitor. Cell. 2020.
385
386
387
388
389

390 **FIGURES AND FIGURE LEGENDS**

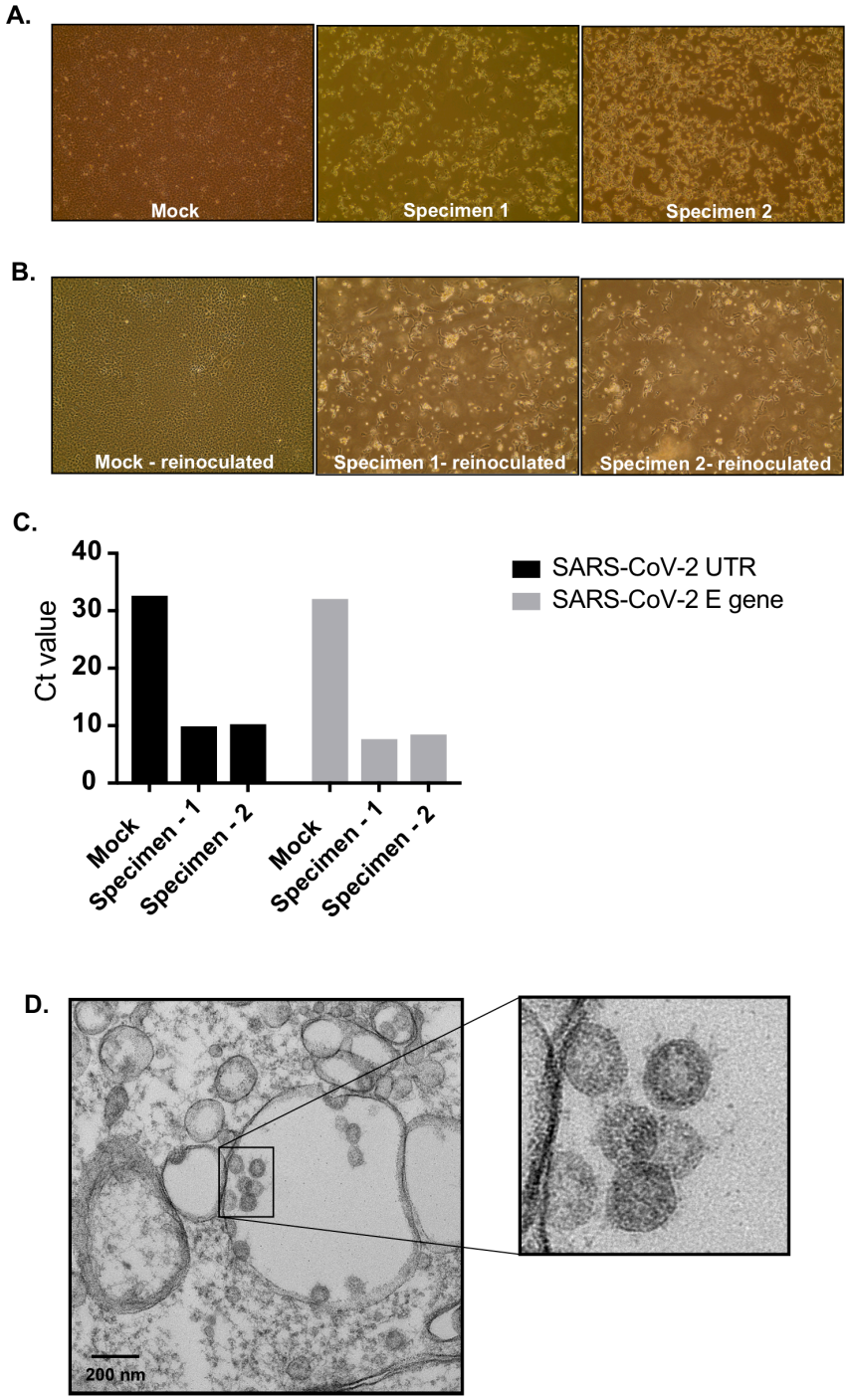

391

392 **Figure 1. Isolating SARS-CoV-2 from COVID-19 patients.** (A) Vero E6 cells were mock

393 inoculated or inoculated with mid-turbinate clinical specimens from COVID-19 patients. Cells

394 were incubated for 72 hours and observed for cytopathic effect (CPE) under a light microscope.

395 (B) To determine if supernatant from Vero E6 cells that were mock inoculated or inoculated with
396 clinical specimens contained replication competent virus, we re-inoculated fresh monolayer of
397 Vero E6 cells and observed cells under a light microscope for CPE after 24 hours. (C)
398 Quantitative real time PCR to detect SARS-CoV-2 5'- untranslated region (UTR) and envelope
399 (E) gene in RNA extracted from supernatant that was collected from Vero E6 cells that were
400 mock infected or infected with COVID-19 clinical specimens for 72 hours. (D) Electron
401 micrograph of Vero E6 cells that were re-infected for 48 hours with supernatant that was
402 collected from Vero E6 cells infected with clinical specimens. Insert – zoomed image of
403 coronavirus-like particles.
404

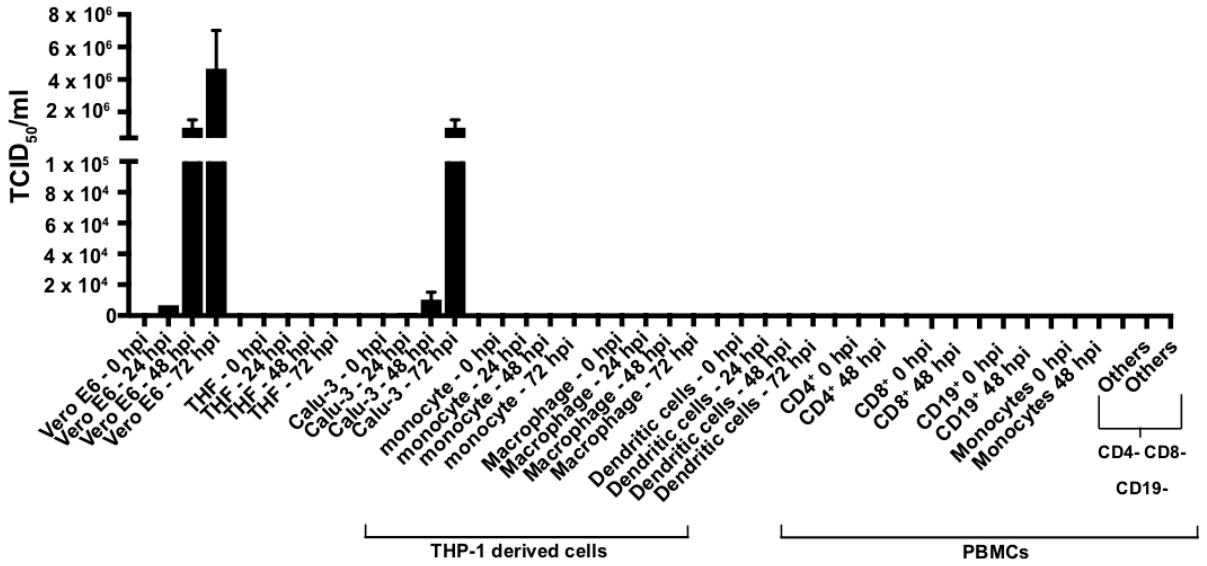

405

406 **Figure 2. Replication of SARS-CoV-2 in human structural and immune cells.** To determine
407 human cells that support SARS-CoV-2 replication, we infected human cell lines and primary
408 cells at an MOI of 0.01 (n = 2 independent experiments; supernatant from each experiment was
409 titrated in triplicates). We infected Vero E6 cells as a control. THF and Calu-3 cells represent

410 human structural cells. THP-1 is a monocyte cell line that was used to derive macrophages and
411 dendritic cells. PBMCs from healthy human donors (n = 2 independent donors) were used to
412 generate $CD4^+$, $CD8^+$, $CD19^+$, monocytes and other ($CD4^-$ $CD8^-$ $CD19^-$) cell populations.
413 Supernatant from infected cells were collected at various times and titrated on Vero E6 cells to
414 determine virus titres ($TCID_{50}$/ml). hpi, hours post infection; CD, cluster of differentiation;
415 PBMC, peripheral blood mononuclear cells.
416

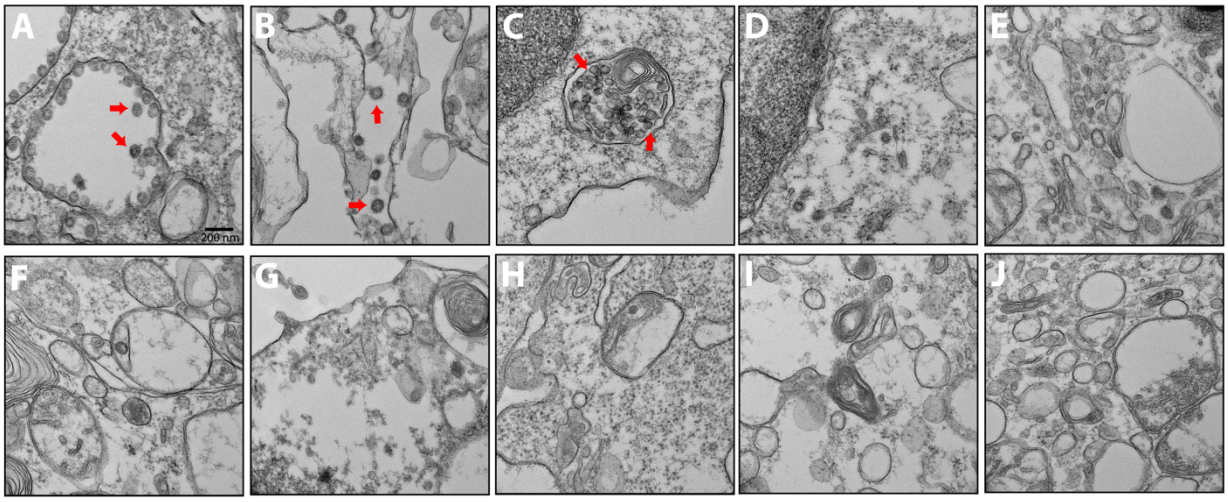

417

418 **Figure 3. Electron micrographs of SARS-CoV-2 infected cells.** To detect coronavirus-like
419 particles in experimentally infected human structural and immune cells, we infected a range of
420 cells with SARS-CoV-2 at a MOI of 0.01 for 48 hours. The cells were fixed, processed and
421 imaged using a transmission electron microscope (n = 10 fields / cell type). Representative image
422 of each cell line is shown above. Virus-like particles are indicated by red arrows. (A) Vero cells.
423 (B) Calu-3 cells. (C) $CD4^+$ PBMC. (D) $CD8^+$ PBMC. (E) $CD19^+$ PBMC. (F) Monocytes from
424 PBMC. (G) Other cells from PBMC ($CD4^-$ $CD8^-$ $CD19^-$ cell populations). (H) THP-1 monocyte.
425 (I) THP-1-derived macrophage. (J) THP-1-derived dendritic cell.
426

427 **TABLE**

Metric or Mutation	SARS-CoV-2/SB2	SARS-CoV-2/SB3_TYAGNC
Number of Paired Reads	730,137 bp	690,167 bp
Reads from SARS-CoV-2	94.0%	94.4%
Number of Assembly Contigs	1	1
Assembly N50	29,494 bp	29,369 bp
Average Depth of Coverage of Reads	7940.0 fold	7550.1 fold
Total Assembly Length	29,494 bp	29,369 bp
SARS-CoV-2 Assembly Completeness	98.6%	98.2%
Unresolved 5' sequence	262 bp	272 bp
Unresolved 3' sequence	200 bp	205 bp
pos. 884 (orf1ab polyprotein)		**R207C (CGT→TGT)**
pos. 1397 (orf1ab polyprotein)	**V378I (GTA→ATA)**	**V378I (GTA→ATA)**
pos. 2832 (orf1ab polyprotein)	K856R (AAG→AGG)	
pos. 3040 (orf1ab polyprotein)		Y925Y (TAC→TAT)
pos. 8327 (or1ab polyprotein)	18.1% of reads suggest L2688F (CTT→TTT)	
pos. 8653 (orf1ab polyprotein)		**M2796I (ATG→ATT)**
pos. 10353 (orf1ab polyprotein)	5.6% of reads suggest K3363T (AAG→ACG)	
pos. 11074 (orf1ab polyprotein)	10.2% of reads suggest +TTT and a deletion between positions 10809 and 13203	
pos. 11083 (orf1ab polyprotein)	**L3606F (TTG→TTT)**	**L3606F (TTG→TTT)**
pos. 25413 (ORF3a protein)		36.7% of reads suggest I7I (ATC→ATT)
pos. 28688 (nucleocapsid phosphoprotein)	**L139L (TTG→CTG)**	**L139L (TTG→CTG)**

428

429 **Table 1. Sequencing read and genome assembly statistics.** Predicted mutations are relative to
430 the MN908947.3 SARS-CoV-2 genome (29,903 bp). Mutations within codons are underlined.
431 All mutations were predicted by 100% of sequencing reads mapping to that position, unless
432 otherwise noted. None of the mutations with support from less than 100% of sequencing reads
433 appeared in the final assembled genome consensus sequences. Substitutions in bold have been
434 observed in direct sequencing of patient isolates (Mubareka & McArthur, unpublished).
435
436
437
438
439
440
441
442
443
444